Environmental Science Nano

Accepted Manuscript

This article can be cited before page numbers have been issued, to do this please use: K. Bodó, Y. Hayashi, G. Gerencsér, Z. László, A. Kéri, G. Galbács, E. Telek, M. Mészáros, M. Deli, B. Kokhanyuk, P. Németh and P. Engelmann, *Environ. Sci.: Nano*, 2020, DOI: 10.1039/C9EN01405E.

ROYAL SOCIETY OF CHEMISTRY

rsc.li/es-nano

View Article Online
DOI: 10.1039/C9EN01405E

Environmental significance statement

Silver and gold nanoparticle-based products have been broadly utilized in both commercial and biomedical fields, and their potential ecotoxicological impacts should be further considered. In particular, harmful effects on the immune systems may result in an undesirable physiological consequence of the exposed organisms. Using macrophage-like cells (coelomocytes) separately harvested from two closely-related *Eisenia* species of earthworms, we compared their biological responses to silver/gold nanoparticles at molecular and cellular levels. Our *in vitro* findings reinforce the existence of species-specific responses towards nanoparticles, which may influence the organism's susceptibility. As nanoparticles behave differently from classical environmental contaminants, additional concerns should be given for species extrapolation from ecotoxicological models to higher or even closely-related organisms.

DOI: 10.1039/C9EN01405E

SPECIES-SPECIFIC SENSITIVITY OF *EISENIA* EARTHWORMS TOWARDS NOBLE METAL NANOPARTICLES: A MULTIPARAMETRIC *IN VITRO* STUDY

Kornélia Bodó[1], Yuya Hayashi[2], Gellért Gerencsér[3], Zoltán László[4], Albert Kéri[5,6], Gábor Galbács[5,6], Elek Telek[7], Mária Mészáros[8], Mária A. Deli[8,9], Bohdana Kokhanyuk[1], Péter Németh[1], Péter Engelmann[1,*]

[1]Department of Immunology and Biotechnology, Clinical Center, Medical School, University of Pécs, Pécs, Hungary

[2]Department of Molecular Biology and Genetics, Aarhus University, Aarhus, Denmark

[3]Department of Public Health Medicine, Medical School, University of Pécs, Pécs, Hungary

[4]Department of Medical Microbiology and Immunology, Medical School, University of Pécs, Pécs, Hungary

[5]Department of Inorganic and Analytical Chemistry, Faculty of Science and Informatics, University of Szeged, Szeged, Hungary

[6]Department of Material Science, Interdisciplanary Excellence Center, University of Szeged, Szeged, Hungary

[7]Department of Biophysics, Medical School, University of Pécs, Pécs, Hungary

[8]Institute of Biophysics, Biological Research Centre, Szeged, Hungary

[9]Department of Cell Biology and Molecular Medicine, University of Szeged, Szeged, Hungary

***Corresponding author:**

Department of Immunology and Biotechnology, Clinical Center, Medical School, University of Pécs, Pécs, H-7643, Szigeti u. 12, Hungary. Tel: + 36-72-536-288, Fax: + 36-72-536-289, email: engelmann.peter@pte.hu

Abstract

Two closely-related earthworm species (*Eisenia* spp.) have long been used as model organisms in ecotoxicology. The same nanoparticles (NPs) may affect the two species differently, not only because of the inherent differences in susceptibility but also due to how immune system could recognize NPs. In a comparative approach using *E. andrei* and *E. fetida*, we study various immune-related parameters of earthworm coelomocytes following *in vitro* exposure to 10 nm NPs (silver, Ag; and gold, Au) or dissolved Ag ($AgNO_3$). In general, *E. fetida* coelomocytes were more susceptible to AgNPs and $AgNO_3$ while AuNPs did not show cytotoxicity. At the sub-cellular level, AgNPs similarly affected cellular redox reactions in both species, however, *E. fetida* showed greater responses for apoptosis-related endpoints. At the molecular level, AgNPs (at 24 h LC_{20}) induced a significantly high level of *superoxide dismutase* in *E. andrei* coelomocytes while *E. fetida* was additionally characterized by consistent induction of *metallothionein* and differential capacity for redox/metal regulation. Although AuNPs were not cytotoxic, both NP types (Ag and Au) seemed to alter the expression pattern of immune-related genes (*toll-like receptor* and *lysenin*) in both species, but more clearly in *E. fetida*. We further observed that lysenin proteins, while secreted differentially between the two species, bind only to AgNPs resulting in negative secretion feedback. Our findings support the general preference of *E. fetida* in ecotoxicology, and reveal the potential roles of protective and immune mechanisms optimized for each species in its own ecological niche.

Keywords: innate immunity, coelomocytes, AgNP, AuNP, apoptosis, gene expression pattern

1. Introduction

Eisenia andrei and *E. fetida* are two closely-related earthworm species widely used in standardized ecotoxicological testing and discerned as separate species by their minor morphological features. In fact, their natural living environment fundamentally indicates dissimilarities in the niche; more specifically, *E. andrei* can be present in manure and compost while *E. fetida* subsists in moist forest soil, however both *Eisenia* spp. frequently constitute mixed colonies[1, 2]. Historically either *E. andrei* or *E. fetida* were used for a given set of experiments[3-5]. This also holds true for the ecotoxicological research on emerging classes of nanomaterials such as silver nanoparticles (AgNPs)[6-10] that could be released to the environment[11]. Even under a controlled experimental setup, however, species differences are indeed considered to be a confounding factor in nanotoxicology due to the formation of species-specific biomolecular coronas potentially in the external milieu (secreted proteins) but also following NP entry into the body (fluid) of an exposed organism[12]. Species differences in the later case have been experimentally proved for earthworms, although only in an artificial *in vitro* setting, where the same NPs with cognate protein corona were preferentially accumulated by immune cells as compared to those with entirely exotic corona formed of fetal bovine serum[13]. Interestingly, the *Eisenia* sp. specific gene *lysenin* has a differential basal expression level between *E. andrei* and *E. fetida*[2, 14], and the encoded protein family was evidently a predominant component of the species-specific protein corona around AgNPs[12]. Despite this emerging paradigm in *Eisenia* earthworms, parallel toxicological and immunobiological studies barely exist to discover the fine differences at certain biological levels of these two closely-related species[2, 15].

Recently the exact genetic distinction between the two species has been solved by species-specific primers for mitochondrial gene cytochrome oxidase (COI) I subunit[2], and this

View Article Online
DOI: 10.1039/C9EN01405E

has made a comparative study possible with a clear genotype. In this work we aimed at exploring species-specific aspects in the stress and immune responses of the two species to 10 nm AgNPs with comparisons to another noble metal NPs (AuNPs) and to dissolved Ag ($AgNO_3$) as a non-NP counterpart. We chose 10 nm AgNPs as model NPs because they are available as an OECD benchmark material for nanotoxicology testing, and we have previously studied several different types/sizes of AgNPs *in vitro* and *in vivo* in *Eisenia* earthworms[10, 12, 16]. In particular, the *in vitro* approach makes the comparison of the two species easier and allows us to focus on the immunologically-relevant mechanistic (rather than ecological) aspects.

Earthworm coelomocytes constitute the cellular arm of innate immunity and are classified into amoebocyte and eleocyte subpopulations, the former of which is considered to be ancestors of vertebrate macrophages[14, 17]. In addition, the coelomic fluid that accommodates coelomocytes possesses a wide range of bioactive molecules (fetidin/lysenin, lysozyme, and lumbricin) that comprise the humoral arm of earthworm immunity[18-21] and are potential opsonins of NPs that could be recognized by the amoebocytes as previously demonstrated[16]. In fact, this would make the amoebocyte subpopulation more susceptible to AgNPs while the dissolved counterpart and heavy metals in general are known to affect both amoebocytes and eleocytes, the latter of which may actually be more vulnerable[8, 9, 22].

The endpoints selected are oxidative stress, DNA damages and apoptosis as well as expression of genes considered as biomarkers of stress and immune responses[10, 12, 16]. This is in line with our choice of NPs; it is generally accepted that oxidative dissolution of AgNPs and thus the release of bioactive Ag ions results in excess reactive oxygen species (ROS) generation leading to DNA damages and apoptotic responses[11, 23, 24]. In contrast, AuNPs may serve as a negative control for these processes since they are highly resistant to oxidative dissolution. They are nonetheless of interest in the context of sub-lethal endpoints as

somewhat inconsistent results have been reported, indicating the unpredictable nature of NP toxicity[25].

Here we ascertained marked contrast of the two earthworm species in the susceptibility of coelomocytes to AgNPs *in vitro*. To the contrary, AuNP exposure had no detectable effects on cell viability of coelomocytes from both species, but it clearly affected gene-, and protein expression of *lysenin*. To the best of our knowledge, this is the first report that describes a direct comparison of earthworm coelomocytes from the two closely-related species *E. andrei* and *E. fetida* on the molecular/cellular toxicity of AgNPs and AuNPs. We further aim to link the *ex situ* lysenin/protein-corona formation and protein secretion to the observed responses of coelomocytes.

2. Materials and methods

2.1. Earthworm husbandry

Adult (clitellated) *E. andrei* and *E. fetida* earthworms were maintained under standard laboratory conditions and collected from breeding stocks[26]. One day before coelomocyte isolations earthworms were placed onto moist tissue paper for depuration to minimize soil contaminations during coelomocyte harvesting. The genotypes of the two species were validated according to Dvořák *et al.,* (2013)[2].

2.2. Extrusion of coelomocytes and *in vitro* exposure conditions

Coelomocytes were separately harvested from *E. andrei* and *E. fetida* earthworm species in the same manner as we described earlier[21] and detailed in the electronic supplementary information (ESI). Following the cell isolations and enumerations (5×10^5 cells), coelomocytes were exposed to different concentrations of NPs (1.25-40 µg/mL) for several time points (1-24 h) in RPMI-1640 cell culture media (with HEPES 3.5 g/L, pH 7.4)

View Article Online
DOI: 10.1039/C9EN01405E

supplemented with 1% penicillin/streptomycin (100 U/mL penicillin and 100 µg/mL streptomycin, Lonza, Basel, Switzerland) and 1% heat-inactivated FBS (Euroclone, Milan, Italy) and placed onto 24-well plates[16]. Where interference is expected in colorimetric measurements, phenol red-free RPMI was used instead. Double-distilled-water (ddH_2O) served as a negative control (in the same volume as the highest concentration of AgNP treatments) and $AgNO_3$ as a positive control for dissolved Ag cytotoxicity[16]. During flow cytometry-based detections only amoebocytes were gated for the analysis as the eleocyte population has a high autofluorescence level.

2.3. Nanoparticles

Polyvinylpyrrolidone (PVP)-capped 10 nm AgNPs and AuNPs (1 mg/mL, BioPure) were purchased from NanoComposix (San Diego, CA, USA) and stored at 4 °C in the dark according to the manufacturer's instructions. Dissolved $AgNO_3$ was purchased from Sigma-Aldrich (Budapest, Hungary).

2.4. Physico-chemical characterization of NPs

Highest applied concentrations of 10 nm AgNP and AuNP (40 µg/mL) was incubated for 24 h at room temperature (RT) in ddH_2O, PBS, RPMI-1640, RPMI-1640 supplemented with 1% FBS. The light absorbance profile (characteristic to the localized surface plasmon resonance of those NPs) was studied by UV/VIS spectrophotometry to determine the aggregation states and particle morphology under exposure conditions. After desalting, particle sizes and morphology of NPs were also investigated at high resolution using a transmission electron microscope (TEM)[16]. The hydrodynamic size and polydispersity index (PdI) of NPs under exposure conditions were determined by a dynamic light scattering (DLS) device (Zetasizer Nano ZS, Malvern Panalytical, Worcestershire, UK). Likewise, zeta

potentials were measured but after three washing steps with ddH_2O (3×20 min, 18 kRCF) to remove serum proteins and minimize electrolyte concentrations[16, 27]. For the quantification of dissolved ion concentrations, NPs were pelleted by ultracentrifugation (1 h, 164-192 kRCF, 4 ^oC) and metal concentrations in the supernatant were analyzed by inductively-coupled plasma mass spectrometry (ICP-MS). More details of the particle characterization are provided in the ESI.

2.5. Concentration-response curve fitting, and the choice of test concentrations

Concentration-response curves were fitted to the results obtained from live/dead cell assays in order to estimate LC_x values for 24 h exposure (see ESI for details). To further study the cytotoxicity mechanisms, we chose a high concentration range for AgNPs (15, 30 and 40 µg/mL) and the highest $AgNO_3$ concentration at which >95% of cells were affected (1.35 µg/mL) to ensure a high signal-to-noise ratio at earlier time points than 24 h. As AuNPs did not induce cytotoxicity at any of the concentrations tested, we chose 20 µg/mL as an intermediate concentration comparable to the AgNP treatments. Where possible, the same live/dead stain 7-AAD (Biotium, Fremont, CA, USA) was used in combination with functional stains in flow cytometry to exclude dead cells or cells with leaky membranes from analysis. For sub-lethal endpoints such as gene and protein expression profiles, we used average LC_{20} values referred to as "low-cytotoxic concentrations" (AgNP: *E. andrei* 2.71 µg/mL and *E. fetida* 2 µg/mL; $AgNO_3$: 0.20 µg/mL) as well as 20 µg/mL AuNP for a comparison.

2.6. Flow cytometric analysis of oxidative, and mitochondrial stress

Following exposure to selected concentrations of AgNP, AuNP or $AgNO_3$, the amoebocyte population of coelomocytes were evaluated for oxidative and mitochondrial

View Article Online
DOI: 10.1039/C9EN01405E

stress parameters (intracellular ROS level, nitric oxide production, caspase-3 activity and mitochondrial membrane potentials) applying cell permeable fluorescent dyes (Biotium) by flow cytometry. Stainings were performed following the manufacturer's instructions and described in details in ESI.

The measurements and data analyses were performed using a FACSCalibur (Beckton Dickinson, Frankin Lakes, NJ, USA) flow cytometer and a FCS Express (DeNovo Software, Glendale, CA, USA) software, respectively.

2.7. Apoptosis detection by TUNEL-assay

To verify apoptosis induction determined by the caspase-3 activity study above, Click-it Plus TUNEL Assay (modified terminal deoxynucleotidyltransferase-dUTP nick end labelling) with Alexa Fluor 488 fluorescent dye (Life Technologies, Carlsbad, CA, USA) was applied to detect the double-stranded DNA-breakage at 24 h exposure. Coelomocytes (80 µL from 5×10^5/mL) were spread onto glass slides using Cytospin 3 (SHANDON, Thermo Scientific, Waltham, MA, USA) apparatus. Slides were dried at RT overnight, before the assay was performed according to the manufacturer's instructions. Cell nuclei were counterstained with 4',6-diamidino-2-phenylindole, dihydrochloride (DAPI, 10 µg/mL, Life Technologies) and then observed using an Olympus BX61 microscope and an AnalySIS software (Olympus Hungary, Budapest).

2.8. Comet assay

To study the DNA damage by Comet assays, coelomocytes (10^6 cells) were exposed for 24 h to AgNPs, AuNPs or $AgNO_3$ or the positive control UV-C for 30 s. Following two washing steps with LBSS (5 min, 100 RCF) alkaline-based sandwich-agarose gel technique was applied on slides according to previous studies[28]. Briefly, Normal Melting Point agarose-

View Article Online
DOI: 10.1039/C9EN01405E

gel (NMA, 0.5%) constituted the first layer and coelomocytes were mixed into the second layer with Low Melting Point agarose gel (LMA, 0.5%), that was covered by another LMA-layer without cells to form the third layer. Thereafter slides were placed in a lysing-solution (1% sodium sarcosinate, 2.5 M NaCl, 100 mM Na_2-EDTA, 1% Triton X-100, 10% DMSO, and 10 mM Tris) for overnight incubation in the dark at 4 °C. The next day, slides were kept in cold electrophoresis buffer (200 mM EDTA, 10 N NaOH, pH: 10) for 20 min. DNA-strains electrophoresis was performed in the same buffer for 40 min at 0.46 mV/cm and 132 mV in the dark. Slides were washed with a neutralizing solution (0.4 M Tris) three times for 5 min and stained with ethidium bromide. At least 80 individual cells were scrutinized from each treatment under an Olympus BX50 fluorescent microscope with 400x magnification and evaluated by an image analysis software (Comet assay IV; Perceptive Instruments Ltd., Bury St Edmunds, UK). Tail Moment values (TM, the extent of the head and tail, size of the head and the strength of fluorescent intensity) were measured for the analysis.

2.9. Gene expression profiling

Coelomocytes were exposed (5×10^5 cells/well) for 2, 12 and 24 h to low-cytotoxic concentrations (LC_{20}) of AgNPs (*E. andrei* 2.71 µg/mL, *E. fetida* 2 µg/mL) or $AgNO_3$ (0.20 µg/mL), or 20 µg/mL AuNP for a comparison as above. Five independent experiments were performed for all conditions. At each time point, coelomocytes were collected and washed twice with LBSS (5 min, 100 RCF). Total RNA extraction and cDNA synthesis were performed following the manufacturer's instructions (High-Capacity cDNA reverse transcription kit, Thermo Scientific) and described in details in ESI, along with the temperature setting used for quantitative real-time PCR (qPCR).

For SYBR Green-based qPCR, the cDNA templates were mixed with gene-specific primer pairs designed using a Primer Express software (Thermo Scientific) and the primer

View Article Online
DOI: 10.1039/C9EN01405E

sequences are summarized in Table S1. The raw fluorescence qPCR data was used to calculate the amplification kinetics and thus the initial quantity of template cDNA (R_0) using DART-PCR[29]. For normalization of the calculated R_0 values, we tested both the conventional housekeeping gene approach (*RPL17* as the internal reference gene) and using the data-driven algorithm NORMA-gene[30]. We opted for the latter approach as it proved more conservative (i.e. minimal influence on the inter-group variation) and effective normalization (i.e. reduction in the intra-group variation). The NORMA-gene normalized R_0 values were then presented relative to the geometric means of the control values at each corresponding time point. Heatmaps were created on $\log_2$-transformed and scaled datasets using the gplots package (ver. 3.0.1.1) in the R environment (ver. 3.5.1.).

For multivariate analyses of the gene expression datasets, principal component analysis (PCA) and correspondence analysis (CA) were performed using the FactoMineR (ver. 1.41)[31] and factoextra (ver. 1.0.5) packages for R. For PCA, the gene expression values were $\log_2$-transformed and scaled. We performed PCA to reduce the dimensionality of the data so as to identify general variations among categories such as species, exposure duration and treatments as well as their combinations. CA was performed without standardization (i.e. scaling) to visualize the treatment-specific gene expression patterns over time.

2.10. Profiling of *ex-situ* protein coronas around nanoparticles

To study the composition of protein coronas around AgNPs and AuNPs, we applied the same methods as described in Hayashi *et al.,* (2013)[12] with some modifications. Briefly, to obtain coelomic proteins (CP) from the coelomocyte culture, the cells (5×10^5 cells/mL) were incubated for 24 h at RT in RPMI cell culture media without serum supplement. The culture medium was then aspirated and centrifuged (5 min, 500 RCF) to remove cells. The supernatants were centrifuged again (10 min, 1700 RCF) and filter-sterilized (through 0.22

µm membrane filters), after which the CP was collected in Protein LoBind tubes (Eppendorf, Hamburg, Germany). According to the earthworm species from which the CP was derived, it was named EaCP or EfCP *(E. andrei* and *E. fetida* coelomic protein, respectively). Total protein concentrations of the CPs were quantified using a BCA-kit (Sigma-Aldrich) and were typically in the range of 250-300 µg/mL. As these concentrations were not high enough to serve as an alternative to 1% FBS (400-600 µg protein/mL), we decided to spike the CP in BSA protein background, achieving a total of 800 µg protein/mL of which 100 µg/mL was CP and 700 µg/mL was BSA. This represents a >5-fold higher protein concentration sufficient to cover the theoretical total surface area of 20 µg of 10 nm AgNPs (106 µg proteins to 11 cm^2 AgNP surface) and 10 nm AuNPs (58 µg proteins to 6 cm^2 AuNP surface). In line with these calculations, we used 1 mL of 20 µg/mL AgNPs and AuNPs. As for the control, we used the same incubation condition without the CP spike. Samples were incubated on an end-over-end rotator for 24 h at RT in the dark, and then were centrifuged for 30 min at 16 kRCF at 21 °C. Supernatants were removed and NPs washed three times with PBS (30 min, 16 kRCF, 21 °C). After the final washing step 2×SDS sample loading buffer was added and samples were boiled for 5 minutes, followed by another centrifugation (30 min, 16 kRCF, 4 °C) to pellet NPs. Supernatants were stored at -80 °C. SDS-PAGE and Coomassie-Brilliant Blue staining were performed as per standard protocols. Reference protein samples were prepared directly from CP (i.e. without incubation with NPs) for comparison with corona proteins on NPs. Images were analyzed with a VilberLourmat Bio-Profil Version 97 gel documentation system (Collégien, France) and a Biocapture Version 12.6 software. In addition, protein identification of excised bands by liquid chromatography combined tandem mass spectrometry (LC-MS/MS) and Western blots (WB) were performed to precisely identify the discrete bands. Specific details of LC-MS/MS measurements and WB are provided in the ESI.

View Article Online
DOI: 10.1039/C9EN01405E

2.11. Analysis of NP-induced protein secretion

Protein secretion profile was examined according to Hayashi *et al*., (2016)[32]. Initially, coelomocytes (5×10^5 cells/sample) were exposed for 4 h and 24 h at RT to the corresponding concentrations of NPs under the same exposure conditions as used in the gene expression study. Vehicle controls were prepared by adding ddH_2O to cells instead of NPs. Following incubations, the culture supernatant (including NPs) was collected into a Protein LoBind tube (Eppendorf), spun down (5 min, 500 RCF) to remove cells and centrifuged again (10 min, 1700 RCF). The total protein concentrations were quantified using a BCA-kit (Sigma-Aldrich) and adjusted to 400-600 µg/mL. SDS sample buffer was added to a small aliquot of the cell-free supernatant and boiled for 5 min. To remove NPs, samples were centrifuged (30 min, 16 kRCF, 4°C), then SDS-PAGE and Coomassie-Brilliant Blue staining was performed as per standard protocols. Image J (NIH) was employed for densitometry analysis.

2.12. Statistical analyses

Each experiment (except qPCR) was repeated three independent times ($n=3$). Statistical analyses were carried out with Prism v5.0 (GraphPad Software, La Jolla, CA, USA). Distribution of normality was overseen prior to additional statistical tests (Shapiro-Wilk Normality Test). All data are presented with the mean and standard error of the mean (SEM). Results were analysed by one-way ANOVA with Kruskal-Wallis test followed by Dunn's post hoc test. The significance level of $\alpha = 0.05$ was applied for all statistical tests.

For qPCR datasets, the relative gene expression values were log-transformed to satisfy the assumption of normality. Student's *t*-test (or Welch's *t*-test where appropriate) was performed in R following Levene's test on the homogeneity of variances. Significant differences between controls and treatments at each time point were determined as $\alpha = 0.05$.

3. Results and discussion

3.1. Physico-chemical characterization of NPs under exposure conditions

Characterization of NPs under the exposure conditions is essential since any biased physico-chemical factors could dramatically influence the cellular response[33]. Even in the high electrolyte and protein-rich milieu, AgNPs revealed a narrow absorbance peak characteristic of localized surface plasmon resonance, suggesting a monodispersed population (Fig. 1a). This was further supported by DLS and TEM (Table 1, Fig. 1c and d), where they also showed a narrow hydrodynamic size distribution, low PdI (Table 1) and no signs of particle aggregation, respectively. AuNPs, on the other hand showed a broader peak in the absorbance spectrum indicating heterogeneity in localized surface plasmon resonance due to the presence of multimeric clusters rather than singly dispersed particles (Fig. 1b). The mean hydrodynamic size and PdI were also a little larger than that of AgNPs (Table1 and Fig. 1c), although the inherent particle size as observed in TEM was smaller (Fig. 1e). These characterization results suggest that, while some degree of protein-induced agglomeration is apparent in AuNPs, the NPs were in general colloidally stable under the exposure conditions used in this study.

Oxidative dissolution of metal NPs, AgNPs in particular, is a critical process that can obscure the NP-specific effects on toxicity as the ionic counterpart is known to be highly bioactive[24]. To address this problem, the dissolved metal ion concentrations were determined by ICP-MS analysis after removal of NPs by ultracentrifugation. The results suggest that oxidative dissolution under the exposure conditions is not a major concern in both NP types, as dissolved fraction was only <0.4% of the total metal mass (Table 1). For the highest concentration of AgNPs used in this study, the dissolved Ag was 0.16 µg/mL, corresponding lower concentration regime used for the $AgNO_3$ treatment.

3.2. Concentration-dependent cytotoxicity is evoked by AgNPs but not AuNPs

We first determined the concentration-response relationship, based on which we selected test concentrations for further analysis on sub-lethal endpoints. Following 24 h exposure to a series of concentrations (1.25-40 µg/mL for AgNPs and AuNPs, 0.05-1.35 µg/mL for $AgNO_3$), the survival rate of coelomocytes was evaluated by 7-AAD, a cell membrane-impermeant nuclear stain. In the flow cytometry analysis, we referred to the amoebocyte population as the surrogates for total coelomocytes, because eleocytes (the other major population of coelomocytes) possess a high riboflavin content that results in strong autofluorescence[1]. On the other hand, a recent study[8] claims that amoebocytes and eleocytes have dissimilar sensitivity towards AgNPs. It is plausible, however, the different cytotoxic response in AgNP-exposed coelomocytes can be explained by the fact that amoebocytes (and not eleocytes) rapidly internalize AgNPs as verified by TEM[16], and thus eleocytes could be affected rather indirectly.

In both earthworm species, AgNP (and $AgNO_3$ at lower concentrations) but not AuNPs exerted concentration-dependent cytotoxicity within the concentration range tested (Fig. S1). This also verifies that the dissolved fraction of AgNPs (<0.4% of total Ag) did not follow the concentration-response curve established for the $AgNO_3$ treatment. As for the species differences, coelomocytes from *E. fetida* showed higher sensitivity towards AgNPs and $AgNO_3$ than *E. andrei* coelomocytes based on the estimated lower LC_x values and the steeper Hill-Slopes (Table S2). Based on the concentration-response curves established here we selected a high concentration series of AgNPs (15, 30 and 40 µg/mL) to study time points earlier than 24 h, and an intermediate AuNP concentration (20 µg/mL) with reference to AgNPs as no changes in the cell viability was observed. For gene and protein expression studies, we opted for low-cytotoxic concentrations (LC_{20}) determined for AgNPs and $AgNO_3$, while AuNPs were tested at the same concentration as above[10].

AgNPs, coincidingly with the literature, exhibited harmful effects on innate immune cells (e.g. earthworm coelomocytes) in low-concentration attributed to their small-size[16, 34]. Contrastingly similar responses were not observed after AuNP treatments (Fig. S1c and d). In this respect, their interactions with biological systems are rather contradictory[35, 36]; however several studies deal with the broad toxicity of AuNPs[37, 38].

3.3. AgNPs induce immediate increase of intracellular ROS, delayed elevation of NO and mitochondrial membrane depolarization

As we hypothesize that oxidative stress is a key process that initiates a cascade of subcellular events upstream of apoptotic determination following exposure to AgNPs, we first evaluated the intracellular level of ROS at early time points (i.e. 1, 2 and 4 h). A concentration-dependent increase in the relative ROS-level was observed for the AgNP treatments (Fig. 2a and b). With regard to the temporal aspect, *E. andrei* coelomocytes showed a peak in the ROS level at 2 h, while *E. fetida* coelomocytes revealed gradual elevation of ROS toward 4 h. Indeed, in general similar trends were observed also for the $AgNO_3$ treatment and positive control (H_2O_2), suggesting an inherent difference in the kinetics of ROS physiology between the two species (Fig. 2a and b).

It has been generally recognized that AgNP exposure results in oxidative stress a process extremely dependent on NP size, shape, dose and duration[24, 39, 40]. A variety of oxidative stress-related abnormalities have been reported for earthworms as well as other invertebrates upon AgNP treatments[16, 41-47], however induction of NO derivates has not been studied in invertebrate immune cells. In the coelomocytes of both *Eisenia* species, the intracellular NO level was slightly higher at 4 h and then strongly increased at 24 h, showing significant differences between the AgNP treatments and the unexposed control (Fig. 2c and

d). Interestingly, $AgNO_3$ did not induce NO production as high as observed for the AgNP treatments, indicating NP-specificity of this response.

In the case of mitochondrial depolarization ($\Delta\psi m$) we did not find any remarkable changes at 4 h in any of the AgNP treatments (Fig. 2e and f). However, at 24 h a significant concentration dependent decrease of mitochondrial membrane potential was observed for *E. fetida* coelomocytes and to a lesser extent for *E. andrei* species.

Taken together, although AgNP induced a similar degree of NO production in the two species, the relative ROS level was rapidly regulated in *E. andrei* coelomocytes resulting in a decreasing trend toward 4 h. On the other hand, the higher degree of mitochondrial stress in *E. fetida* coelomocytes may reflect the lower survival of cells compared to *E. andrei* species (Table S2). The positive correlation of mitochondrial depolarization and cell death was also evident for the $AgNO_3$ treatments, underscoring that the former process is linked to subsequent cell death[48]. We do not know whether the intracellular ROS level could have been much higher in *E. fetida* coelomocytes at 24 h than the earlier time points tested here, as the measurement of ROS levels becomes more complicated when the cells are under stress. Interesting to note is that in the hemocytes of *Mytilus galloprovincialis* AgNPs did not cause elevated ROS levels but the mitochondrial membrane potential was significantly decreased[48], as was the case for *E. fetida* coelomocytes in this study. It is nonetheless plausible that the cellular redox balance (indicated by the excess ROS level) was affected at initial stages of AgNP and $AgNO_3$ exposure, as a consequence of which mitochondrial membrane depolarization persisted for long enough to trigger cell death in both treatments at 24 h. As $AgNO_3$ did not significantly altered the intracellular NO level unlike AgNPs, this process deserves a further investigation that may provide insights into the NP-specific modes of cellular responses. In all cases, as predicted from the cytotoxicity assays, AuNPs did not induce any of the changes in coelomocytes of both species.

3.4. AgNPs induce caspase-3 activation and DNA damages

To further strengthen our hypothesis outlined above, we next focused on the parameters directly linked to apoptosis. As expected, a concentration-dependent caspase-3 activity was noted in the AgNP treatment in both species, in particular in *E. fetida* coelomocytes that showed a significant difference at the highest concentration at 24 h (Fig. 3a and b). $AgNO_3$ induced higher caspase-3 activity already at 4 h and then at 24 h in both species. The AuNP treatments again did not show any notable changes. Of particular interest is the general weaker response of *E. andrei* coelomocytes compared to *E. fetida*. The molecular signature of apoptosis was further indicated by TUNEL assays revealing double strand DNA breaks in AgNP and $AgNO_3$ treatments (Fig. 3c and d). TUNEL assay controls and the concentration series of AgNPs validated the assay specificity (Fig S3a and b). These observations are all in line with the cytotoxicity and the mitochondrial depolarization results. By means of TUNEL assay a previous study[49] has reported that AgNP treatments caused DNA damages in THP-1 monocytic cell line which could be linked to excess ROS production. Furthermore, in rat hippocampus AgNPs induced apoptosis in a dose-dependent manner observed by TUNEL staining[50]. Likewise Ribeiro *et al.,* (2019)[51] documented apoptosis of *E. fetida* coelomocytes upon copper oxide nanomaterial exposure *in vitro*.

As another method of choice for sensitive detection of single/double-stranded DNA breakage, Comet-assay is a widely applied method including the genotoxicity evaluation of NPs in individual cells[52]. Following 24 h exposure, at which we were able to detect significant caspase-3 activation (Fig. 3), AgNPs triggered concentration-dependent genotoxic effects in coelomocytes of both species (Fig. 4). Furthermore, we noted higher TM-values in *E. fetida* coelomocytes compared to *E. andrei* after exposure to AgNPs or $AgNO_3$ (Fig. 4a). In support of our findings, another study[42] on AgNP genotoxicity revealed concentration-dependent appearance of micronuclei and bi-nucleated coelomocytes of *Aporrectodea caliginosa*

View Article Online
DOI: 10.1039/C9EN01405E

earthworms. As a side note, while we did not find any changes in the AuNP-exposed coelomocytes, by Comet assays Lopez-Chaves *et al.,* (2018)[37] observed DNA-damage caused by AuNPs in a size-dependent manner (10, 20, 30, and 60 nm) in HepG2 hepatoma cells.

3.5. Identification of species-independent features in gene responses to AgNPs

To further gain insights into the species differences in sensitivity towards noble metal NPs, we analyzed expression profiles of several target genes (stress-related: *superoxide-dismutase-SOD*, *metallothionein-MT,* pattern-recognition receptor (PRR): *toll-like receptor-TLR,* and antimicrobial peptide genes: *lysenin*, *lumbricin*, *lumbricin-related peptide-LuRP*) in a multiparametric manner: two different species, time kinetics (2, 12 and 24 h) and various treatments (AgNP, AuNP, and $AgNO_3$). Low-cytotoxic concentrations (LC_{20} values) of AgNPs (*E. andrei:* 2.71 µg/mL and *E. fetida:* 2 µg/mL), and $AgNO_3$ (0.20 µg/mL for both species) were selected for the experiments to standardize the concentration-response relationship between the two species. For AuNPs, the non-cytotoxic concentration (20 µg/mL) was used as above.

To explore the general patterns, we first visualized the datasets in a heatmap for each species based on z-scores and thus treating all genes equally independent of the inherent expression levels. Relative expression profiles of *E. fetida* have a broader z-score distribution and the resulting heatmap features more extreme values than the heatmap for *E. andrei* in which expression values around the mean (z-score of zero) are found more frequently (Fig. 5a). This suggests in general that *E. fetida* coelomocytes are more sensitive to the studied treatments. Using z-transformed datasets, PCA was performed to identify global patterns specific to species, treatments or time points, or the combinations of the latter two (treatment × time). In all cases, the first two PCs explained >50% of the total variations. Despite the global difference in the degree of transcriptional responses (Fig. 5a), the overall gene

expression patterns were not largely different between the two species (Fig. S3a). Expression patterns likely common to both species were observed with samples having negative PC1 scores; they are weakly represented by the AgNP and $AgNO_3$ treatments (Fig. S3b, mean points labelled in yellow and blue, respectively) and by 24 h (Fig. S3c, mean point labelled in orange), but clearly indicated when the treatments and the time point were combined (i.e. 24 h exposure to AgNPs or $AgNO_3$) (Fig. 5b, mean points labelled in brownish yellow and dark blue, respectively). The gene contributing largely to PC1 (strongly related to AgNP and $AgNO_3$ treatments at 24 h) is *lysenin* due to relatively low expression levels, while *SOD* and *MT* have influences over PCs 1 and 2 mainly as a result of relatively high expression levels (Fig. 5b). Overall with respect to the effect of treatments and time points, PCA identified the 24 h time point for AgNP and $AgNO_3$ treatments as characteristically different from the rest, and the difference stemmed from the expression patterns of *lysenin* and *SOD* common to both *E. andrei* and *E. fetida* possibly indicating a general stress response pattern in *Eisena* spp.

3.6. Exploration of time- and treatment-specific gene expression patterns

In contrast to PCA, CA is a more direct approach to visualize the multidimensional datasets in simpler plots without z-transformation. This makes the interpretation easier when the temporal aspects of two treatments are compared (Fig. 5). CA can thus identify common and uncommon characteristics among the two species focusing on the correspondence between time and gene response patterns. For a reference, results from the univariate statistics are presented in Fig. S4. In CA, we directly compared AgNP datasets to AuNP or $AgNO_3$ to explore features specific to NPs or $AgNO_3$, respectively. In general to both of *E. andrei* and *E. fetida*, the two genes *lysenin* and *MT* had the highest contributions in the opposite direction to the first axis (Dimension 1) that explains >50% of the variations of the data analyzed (Fig. 6). This reflects the tendency common to both species, as identified in PCA, that *lysenin* is

View Article Online
DOI: 10.1039/C9EN01405E

induced when *MT* is down-regulated and that the relative expression levels of these two genes are more pronounced than other genes tested. Intriguingly, the second axis (Dimension 2) appears to characterize the temporal aspects. In *E. andrei lysenin* is on the opposite side of *SOD* and *TLR*, with *MT* localized in the middle, where *lysenin* is positively correlated with the 2 h profiles, and *MT* with the 12 h profiles (Fig. 6a and 6c). Of particular note is that the AgNP treatment and to a lesser extent the AuNP treatment were also negatively correlated with *lysenin* and positively with *SOD*/*TLR* at the 24 h time point. What this tells us is that, irrespectively of the treatment types, *lysenin* was induced at 2 h and down-regulated towards 24 h, while *MT* was induced when *lysenin* expression was at the baseline level at 12 h. In the AgNP/AuNP treatments, concurrent with the suppression of *lysenin* at 24 h (AgNP, $p = 0.002$; AuNP, $p = 0.039$), induction of *SOD* (AgNP, $p = 0.006$) and *TLR* became apparent (Fig. S4a). In *E. fetida*, on the second axis *MT* is now closer to *lysenin*, being opposite to *SOD* and *TLR* (Fig. 6b and 6d). Unlike *E. andrei*, the induction of *TLR* by AgNP and AuNP was observed at 2 h (AgNP, $p = 0.022$; AuNP, $p = 0.020$), while it was not affected by $AgNO_3$ (Fig. S4b). The comparison between the AgNP and $AgNO_3$ treatments revealed some similarity in the expression profiles, except that there was a fair contribution of *LuRP* to the second axis in general pushing the $AgNO_3$ profiles to negative scores (Fig. 6d). Apart from *LuRP*, both treatments were mainly characterized by suppression of *lysenin* at 2 h ($AgNO_3$, $p = 0.005$) and 24 h (AgNP, $p \leq 0.001$; $AgNO_3$, $p = 0.003$), and gradual induction of *MT* towards 24 h (AgNP, $p = 0.006$; $AgNO_3$, $p \leq 0.001$) (Fig. S4b). As identified in PCA, common to both species is that AgNPs down-regulated *lysenin* at 24 h concurrent with induction of *SOD* and additionally *MT* in the case of *E. fetida*. Gene responses to AgNPs and $AgNO_3$ showed similar patterns in both species with some exceptions possibly due to large biological variations in the genes such as *MT* and *LuRP* (see the controls in Fig. S4).

As another factor that differentiated between the two species, basal expression levels of the genes *lumbricin, lysenin* and *SOD* were higher in *E. andrei*, whereas *TLR, LuRP* and *MT* in *E. fetida* were highly inducible under stress conditions (Table S3). Temporal expression profiles shed further light on that *E. fetida* coelomocytes are undoubtedly more sensitive to the examined treatments (Fig. 5a), but between the two species the complete gene expression patterns were not entirely distinguished (Fig. S4a). As previously observed in *E. fetida*, *MT* and *lysenin* regulation changed rapidly by environmental stressors, therefore it is considered to be an early biomarker of stress[53]. Consistent with our results, Hayashi *et al.,* (2016)[32] observed *MT* induction and opposing down-regulation of *lysenin* over time following 2-24 h exposure of *E. fetida* coelomocytes to AgNPs (NM-300K, 15 nm) and $AgNO_3$ that bear out the use of these genes as biomarkers upon metal burdens[53]. Not only *MT* but also the increasing expression of *SOD* in both species also suggests the onset of oxidative stress response, characterized by activation of the anti-oxidative defense system in cooperation with quenching of thiol-reactive metals. In particular, *SOD* is responsible for the attenuation of free superoxide radicals, and its up-regulation was documented for mice lung tissues exposed to AgNPs[54]. Similar phenomena were observed after exposure of human hepatoma cells to AgNPs[55].

Furthermore, early induction (at 2 h) of the *TLR* in *E. fetida* is possibly a result of the macrophage-like cells interacting with NPs[32, 56]. Upon PRR engagement by NPs, it is plausible that antimicrobial peptides expression is increased, however, our findings revealed that *lumbricin* and *LuRP* mRNA expression had a rather constitutive pattern following pathogen treatment in *E. andrei* coelomocytes[18, 32].

Although we did not observe cytotoxicity of AuNPs at the concentration used, significantly differential expression patterns were evidenced for *TLR*, *lysenin* and *MT* (Fig. S4), possibly indicating mechanisms that are not directly related to cell death but rather the

interactions with NPs. For instance, in *Sparus aurata* fish AuNPs altered expression of genes involved in antioxidant and innate immune responses while not affecting expression of *sod*[57]. The potential impact of AuNPs on innate immunity is therefore a topic that may deserve further attention upon establishment of dose-response relationship on an immune-related parameter, not cytotoxicity.

3.7. AgNPs preferentially interact with lysenins and regulate their secretion under exposure conditions

We have previously documented the species-specific formation of protein coronas using *E. fetida* coelomic proteins (EfCP), where the family of lysenin proteins showed characteristic enrichment at both 15 and 75 nm AgNPs[12]. On the other hand, the properties of neither *E. andrei* coelomic proteins (EaCP) nor the combination with AuNPs' have been investigated yet. Since basal gene expression level of lysenin is different in *Eisenia* spp.[2, 58], with a particular focus of lysenins we hereby analyzed the compositions of protein coronas to identify proteins that have high affinity for AgNP but also for AuNPs. As previously performed, EaCP and EfCP were harvested after incubating coelomocytes in culture media without serum supplement. In this study, however, we used BSA as a background protein source to ensure a high protein concentration enough to prevent protein-induced agglomeration of NPs. This approach also emphasizes the specificity of NP-protein interactions in the same way as immunostaining where BSA or milk proteins are commonly used for blocking non-specific binding. Indeed, despite the high abundance of BSA (66 kDa bands) in the incubation mix ("Reference"), enrichment of CP-specific proteins (38, 40 and 45 kDa bands) were observed for protein coronas formed around AgNPs or AuNPs (Fig. 7a). The minor interactions of both AgNPs and AuNPs with BSA were also evident as there were only

little differences in the band intensities for BSA between the CP-spiked samples and "No-spike" controls (Fig. 7a).

Previously, we have shown the specificity of lysenin, a major protein component of EfCP, in the interaction with AgNPs and not with silica NPs[12]. In this study, we used AuNPs for a comparison as they have a similar chemical property with AgNPs in terms of the surface reactivity with thiols. To our surprise, the Western blot analysis rather proved that binding of lysenins (38 kDa and 40 kDa bands) is restricted to AgNPs, excluding the possibility for thiol-driven interactions (Fig. 7a). Surface hydrophobicity could contribute to the preferential binding of lysenins, as discussed earlier[12]. As for the species differences, we have noted a clear difference in lysenin proteins (38 kDa and 40 kDa bands) between EaCP and EfCP, and thus the resulting protein coronas around AgNPs (Fig. 7a, Western blot, also marked with red arrows in the SDS-PAGE gel).

To identify these proteins as well as the 45 kDa proteins that were enriched both by AgNPs and AuNPs, we performed LC-MS/MS following excision of those bands (from both species but only the bands representing corona proteins associated with AgNPs). This verified the identity of the proteins from the lysenin family (lysenin and lysenin-related protein 2; LRP2), whereas the 45 kDa bands were likely represented by actin (Table S4). As we detected both lysenin and LRP2 to the same extent in the 38 and 40 kDa bands from both species, it could be that the 40 kDa band corresponds to LRP2 (also named as fetidin), a slightly larger variant of lysenin. Unfortunately, it was not possible to confirm this because the two lysenin proteins share a high similarity in amino acid sequence (89% identity) and thus no distinction was made for the 40 kDa band observed in *E. andrei*, where only single band was visible for the lysenin proteins.

In addition to the lysenin protein family, actin is also a constituent of protein coronas formed around AgNPs[12]. Although actin is considered as cytosolic proteins, its putative role

as a secreted, extracellular protein is also emerging for invertebrate organisms. For example, extracellular actin from cell-free hemolymph is able to attach to the surface of diverse bacterial strains[59]. Alijagic *et al.,* (2019)[60] have also identified actin in the complex protein corona on titanium-dioxide NPs after *in vitro* exposure of sea urchin immunocytes. It is thus plausible that earthworm extracellular actin may possess an analogous role with actin of insects, gastropods and echinoderms (e.g. mediating phagocytosis and killing bacteria)[60, 61]. As the binding of actin was likely the case for both AgNPs and AuNPs, future studies may benefit from characterization of extracellular actin in the context of innate immunity in particular in relation to pattern recognition mechanisms. Nevertheless, this study has provided an experimental evidence that species differences at NPs can manifest even for a pair of closely-related species due to the inherent difference in the protein repertoire. The specific enrichment of lysenins at AgNPs despite the high BSA background also signifies that a similar result can be assumed for the exposure conditions used here in other cell assays (i.e. culture media supplemented with 1% FBS), as we previously demonstrated using a larger size of AgNPs[12]. As this assumption is largely influenced by the secretion level of lysenins *in situ*, we next tested the effects of AgNPs and AuNPs on the lysenin secretion profile.

We have previously investigated the protein secretion profile of *E. fetida* coelomocytes treated with a low-cytotoxic concentration of 15 nm AgNPs and observed an apparently higher level of lysenin secretion at 2 h that consistently decreased towards 24 h[32]. In the present study, we applied the same methodology but with additional confirmation by Western blotting in an attempt to compare with the differential expression profile of the *lysenin* gene. We first confirmed that the lysenin secretion in the controls was in the same range as the concentration of lysenins in the CP-spiked "Reference protein" controls (Fig. 7b and c), validating the relevance of the *ex situ* protein corona profiling study (Fig. 7a). Notably for both earthworm species, exposure to AgNPs or AuNPs initially resulted in higher

secretion of lysenins at 4 h compared to the controls (Fig. 7b and c). Subsequently, the amount of lysenins diminished at 24 h (Fig. 7b and c) concurrently with down-regulation of the gene (except for the 24 h exposure of *E. fetida* coelomocytes to AuNPs) (Fig. S4). This indicates that the secretion profile of lysenins generally follows the pattern of the differentially expressed *lysenin* gene, and that even without the CP-spikes the formation of lysenin-rich protein coronas on AgNPs may take place in the presence of coelomocytes. As the regulation of the gene and secretion of the protein were in general common to both AgNPs and AuNPs, in addition to the significant impact of $AgNO_3$ on the gene expression, lysenins are likely stress-regulated proteins that have immunological functions.

Given its putative role for AgNP uptake in coelomocytes[12], the family of lysenin proteins may represent a non-mammalian translation of acute-phase reactions that could affect the kinetics of NP uptake via a negative feedback loop *in vitro* and *in vivo* in *Eisenia* earthworms.

Conclusions

The interaction of NPs and immune systems is poorly understood, in particular in invertebrate models as NPs may acquire a rather species-specific biological identity that is largely different from the well-studied mammalian models[12]. This emerging aspect of NPs adds another dimension to the susceptibility of the exposed organisms in the environment that is primarily represented by chemical tolerance. Demonstrated in the present study is the differential sensitivity to noble metal NPs in coelomocytes of two closely-related earthworm species that have been historically used in ecotoxicological studies. In general, *E. fetida* coelomocytes showed greater sensitivity to AgNPs compared to *E. andrei*, whereas we could not determine species sensitivity to AuNPs for the concentration range tested. The higher cell death at 24 h in *E. fetida* was also supported by the higher degree of apoptosis-related sub-

View Article Online
DOI: 10.1039/C9EN01405E

cellular events such as mitochondrial membrane depolarization, caspase-3 activation and DNA damages at 24 h. Exception was the intracellular redox balance represented by ROS and NO levels, where both *Eisenia* spp. showed responses to a similar extent or possibly even more prominent in *E. andrei* revealing rapid quenching of excess ROS by 4 h. The gene expression profiles indeed suggest involvement of antioxidant mechanisms such as *SOD* in both species, and persistent up-regulation of *MT* in *E. fetida* underscoring the thiol-mediated detoxification process towards 24 h. Furthermore, rapid regulation of an immune-related gene (*TLR*) was evident in *E. fetida* coelomocytes as an NP-specific response common to AgNPs and AuNPs, which may not be related to redox/cytotoxicity but rather to cellular interactions at the initial phase of exposure. In both species, expression/secretion of lysenins seems to be stress-regulated and this implies a complex feedback mechanism for AgNPs because lysenins are specifically enriched by AgNPs and known to enhance uptake by earthworm coelomocytes.

One possible explanation for the higher responsiveness of *E. fetida* is that its natural living environment is considerably different from that of *E. andrei*. Specifically, *E. andrei* flourishes in microbe-rich compost while *E. fetida* subsists in moist forest soil, underlining genetic alterations in sensibility, susceptibility, as well as tolerance of their immune system evolved through natural selection[2]. Our findings reveal the preference of *E. fetida* in contrast to *E. andrei* in immuno-toxicological studies on nanomaterials not only because of the species sensitivity identified in this study but also it better represents the soil ecosystem as a keystone species.

Acknowledgements

We are grateful to Dr. László Molnár and Dániel Dunai (Faculty of Sciences, University of Pécs) for providing earthworm specimens. We would like to thank the help of

View Article Online
DOI: 10.1039/C9EN01405E

Prof. Dr. László Seress and Tünde Faragó (University of Pécs) for sample preparation and TEM imaging. We are also grateful to Emese Papp, Gréta Tolnai, László Girán (University of Pécs) for their technical assistance and to Dr. Éva Csősz, Dr. Zsolt Czimmerer (Univerity of Debrecen) and for Dr. Mirna Velki (Josip Juraj Strossmayer University, Croatia) for their help. We acknowledge the financial support to Medical School Research Foundation University of Pécs (PTE-ÁOK-KA 2017/4), GINOP-232-15-2016-00050, EFOP-361-16-2016-00004. The work was supported by the ÚNKP-19-3-I New National Excellence Program of the Ministry for Innovation and Technology to KB, the János Bolyai Research Scholarship of the Hungarian Academy of Sciences to PE and by Lundbeck Foundation through a post-doctoral fellowship (R219-2016-327) given to YH. Electron microscopic studies were funded by the grant GINOP-2.3.3-15-2016-0002. Mass spectrometry analysis was carried out at the BMBI Proteomics Core Facility, University of Debrecen. The Orbitrap Fusion mass spectrometer was provided by grant: GINOP-2.3.3-15-2016-00020 for the Proteomics Core Facility. GG and AK kindly acknowledge the financial support received from grants EFOP-3.6.2-16-2017-00005 and TUDFO/47138-1/2019 (ITM FIKP program).

Author contributions

Conceptualization and experimental design: KB, YH, EP. Performing experiments: KB, EP, GG, ZL, AK, ET, MM. Data analysis: KB, YH, EP. Reagents/tools/technical assistance: KB, YH, EP, GG, MD, BK, PN. Writing manuscript: KB, YH, EP.

References

1 A. Rorat, N. Kachamakova-Trojanowska, A. Jozkowicz, J. Kruk, C. Cocquerelle,F. Vandenbulcke, M. Santocki, and B. Plytycz, Coelomocyte-derived fluorescence and DNA markers of composting earthworm species, *J. Exp. Zool. A. Ecol. Genet. Physiol.,* 2014, **321**, 28-40.

2 J. Dvořák, V. Mančíková, V. Pižl, D. Elhottová, M. Silerová, R. Roubalová, F. Skanta, P. Procházková, and M. Bilej, Microbial environment affects innate immunity in two closely related earthworm species *Eisenia andrei* and *Eisenia fetida*, *PLoS One*, 2013, **8**, e79257.

3 D. J. Spurgeon, and S. P. Hopkin, Effects of metal- contaminated soils on the growth, sexual development, and early cocoon production of the earthworm *Eisenia fetida*, with particular reference to zinc, *Ecotoxicol. Environ. Saf.* 1996, **35**, 86-95.

4 S. Sauvé, and M. Fournier, Age-specific immunocompetence of the earthworm *Eisenia andrei*: exposure to methylmercury chloride, *Ecotoxicol. Environ. Saf.,* 2005, **60**, 67-72.

5 S. Ečimović, M. Velki, R. Vuković, I. Štolfa Čamagajevac, A. Petek, R. Bošnjaković, M. Grgić, P. Engelmann, K. Bodó, V. Filipović-Marijić, D. Ivanković, M. Erk, T. Mijošek, and Z. Lončarić, Acute toxicity of selenate and selenite and their impacts on oxidative status, efflux pump activity, cellular and genetic parameters in earthworm *Eisenia andrei*, *Chemosphere,* 2018, **212**, 307-318.

6 J. I. Kwak, M. W. Lee, S. W. Kim, and Y. L. An, Interaction of citrate-coated silver nanoparticles with earthworm coelomic fluid and related cytotoxicity in *Eisenia andrei*, *J. Appl. Toxicol.* 2014, **34**, 1145-1154.

7 K. Schlich, T. Kiawonn, K. Terytze, and K. Hund-Rinke, Effects of silver nanoparticles and silver nitrate in the earthworm reproduction test, *Environ. Toxicol. Chem*. 2013, **32**, 181-188.

8 N. Garcia-Velasco, A. Irizar, E. Urionabarrenetxea, J. J. Scott-Fordsmand, and M. Soto, Selection of an optimal culture medium and the most responsive viability assay to assess AgNPs toxicity with primary cultures of *Eisenia fetida* coelomocytes, *Ecotox. Env. Saf.,* 2019, **183,** 109545, doi: 10.1016/j.ecoenv.2019.109545.

9 N. Garcia-Velasco, A. Pena-Cearra, E. Bilbao, B. Zaldibar, and M. Soto. Integrative assessment of the effects produced by Ag nanoparticles at different levels of biological complexity in *Eisenia fetida* maintained in two standard soils (OECD and LUFA 2.3). *Chemosphere*, 2017, **181**, 747-758.

10 Y. Hayashi, L. H. Heckmann, V. Simonsen, and J.J. Scott-Fordsmand, Time-course profiling of molecular stress responses to silver nanoparticles in the earthworm *Eisenia fetida*, *Ecotox. Env. Saf.,* 2013, **98**, 219-226.

11 P. S. Tourinho, C. A. van Gestel, S. Lofts, C. Svendsen, A. M. Soares, and S. Loureiro, Metal-based nanoparticles in soil: fate, behavior, and effects on soil invertebrates, *Environ. Toxicol. Chem.,* 2012, **31**, 1679-1692.

12 L. Canesi, T. Balbi, R. Fabbri, A. Salis, G. Damonte, M. Volland, and J. Blasco, Biomolecular coronas in invertebrates: implications in the environmental impact of nanoparticles, *Nanoimpact*, 2017, **8**, 89-98.

13 Y. Hayashi, T. Miclaus, C. Scavenius, K. Kwiatkowska, A. Sobota, P. Engelmann, J. J. Scott-Fordsmand, J. J. Enghild, and D. S. Sutherland, Species differences take shape at nanoparticles: protein corona made of the native repertoire assists cellular interaction, *Environ. Sci. Technol.,* 2013, **47**, 14367-14375.

14 P. Engelmann, Y. Hayashi, K. Bodó, and L. Molnár, in *Lessons in immunity: from single cell organism to mammals,* ed. L. Ballarin and M. Cammarata, Elsevier, Amsterdam, 1stedn., 2016, ch. 4, pp 53-66.

15 H. Suleiman, A. Rorat, A. Grobelak, A. Grosser, M. Milczarek, B. Plytycz, M. Kacprzak, and F. Vandenbulcke. Determination of the perfomance of vermicomposting process applied to sewage sludge by monitoring of the compost quality and immune responses in three earthworm species: *Eisenia fetida*, *Eisenia andrei* and *Dendrobaena veneta*, *Bioresour. Technol.*, 2017, **241**, 103-112.

16 Y. Hayashi, P. Engelmann, R. Foldbjerg, M. Szabó, I. Somogyi, E. Pollák, L. Molnár, H. Autrup, D. S. Sutherland, J. J. Scott-Fordsmand, and L. H. Heckmann, Earthworms and humans *in vitro*: characterizing evolutionarily conserved stress and immune responses to silver nanoparticles, *Environ. Sci. Technol.,* 2012, **46**, 4166-4173.

17 E. L. Cooper, E. Kauschke, and A. Cossarizza, Digging for innate immunity since Darwin and Metchnikoff, *Bioessays,* 2002, **24**, 319-333.

18 K. Bodó, Á. Boros, É. Rumpler, L. Molnár, K. Böröcz, P. Németh, and P. Engelmann, Identification of novel lumbricin homologues in *Eisenia andrei* earthworms, *Dev. Comp. Immunol.,* 2019, **90**, 41-46.

19 R. Josková, M. Silerová, P. Procházková, and M. Bilej, Identification and cloning of an invertebrate-type lysozyme from *Eisenia andrei*, *Dev. Comp. Immunol.,* 2009, **33**, 932-938.

20 P. Procházková, M. Silerová, J. Felsberg, R. Josková, A. Beschin, P. De Baetselier, and M. Bilej, Relationship between hemolytic molecules in *Eisenia fetida* earthworms, *Dev. Comp. Immunol.,* 2006, **30**, 381-392.

21 P. Engelmann, L. Pálinkás, E. L. Cooper, and P. Németh, Monoclonal antibodies identify four distinct annelid leukocyte markers, *Dev. Comp. Immunol.,* 2005, **29**, 599–614.

22 A. Irizar, C. Rivas, N. Garcia-Velasco, F. Goni de Cerio, J. Etxebarria, I. Marigómez, and M. Soto, Establishment of toxicity thresholds in subpopulations of coelomocytes

(amoebocytes vs. eleocytes) in *Eisenia fetida* exposed in vitro to a variety of metals? implications for biomarker measurements, *Ecotoxicol*. 2015, **24**, 1004-1013.

23 M. A. Zoroddu, S.Medici, A. Ledda, V. M. Nurchi, J. I. Lachowicz, and M. Peana, Toxicity of nanoparticles, *Curr. Med. Chem.,* 2014, **21**, 3837-3853.

24 L. L. Maurer, and J. N. Meyer, A systematic review of evidence of silver nanoparticle-induced mitochondrial toxicity, *Env. Sci. Nano,* 2016, **3**, 311-322.

25 C. Tao, Antimicrobial activity and toxicity of gold nanoparticles: research progress, challenges and prospects, *Lett. Appl. Microbiol.,* 2018, **67**, 537-543.

26 L. Molnár, P. Engelmann, I. Somogyi, L. L. Mácsik, and E. Pollák, Cold-stress induced formation of calcium and phosphorous rich chloragocyte granules (chloragosomes) in the earthworm *Eisenia fetida*, *Comp. Biochem. Physiol. A. Mol. Integr. Physiol.,* 2012, **163**, 199-209.

27 M. Mészáros, G. Porkoláb, L. Kiss, A. M. Pilbat, Z. Kóta, Z. Kupihár, A. Kéri, G. Galbács, L. Siklós, A. Tóth, L. Fülöp, M. Csete, Á. Sipos, P. Hülper, P. Sipos, T. Páli, G. Rákhely, P. Szabó-Révész, M. A. Deli, and S. Veszelka, Niosomes decorated with dual ligands targeting brain endothelial transporters increase cargo penetration across the blood-brain barrier, *Eur. J. Pharm. Sci.,* 2018, **15**, 228-240.

28 G. Gerencsér, K. Szendi, K. Berényi, and C. Varga, Can the use of medical muds cause genotoxicity in eukaryotic cells? A trial using comet assay, *Environ. Geochem. Health,* 2015, **37**, 63-70.

29 S. N. Peirson, J. N. Butler, and R. G. Foster, Experimental validation of novel and conventional approaches to quantitative real-time PCR data analysis, *Nucleic Acids Res.,* 2003, **31**, e73.

30 L. H. Heckmann, P. Sorensen, P. Krogh, and J. Sorensen, NORMA-Gene: A simple and robust method for qPCR normalization based on target gene data, *BMC Bioinformatics,* 2011, **12**, 250.

31 S. Le, J. Josse, and F. Husson, FactoMineR: An R package for multivariate analysis, *Journal of Statistical Software,* 2008, **25**, 1-18.

32 Y. Hayashi, T. Miclaus, P. Engelmann, H. Autrup, D. S. Sutherland, and J. J. Scott-Fordsmand, Nanosilver pathophysiology in earthworms: Transcriptional profiling of secretory proteins and the implication for the protein corona, *Nanotoxicology,* 2016, **10**, 303-311.

33 B. S. Zolnik, A. González-Fernandez, N. Sadrieh, and M. A. Dobrovolskaia, Nanoparticles and the immune system, *Endocrinology,* 2010, **151**, 458-465.

34 M. J. van der Ploeg, R. D. Handy, P. L. Waalewijn-Kool, J. H. Van den Berg, Z. E. Herrera Rivera, J. Bovenschen, B. Molleman J. H. Baveco, P. Tromp, R. J. Peters, G. F. Koopmans, I. M. Rietjens, and N. W. van den Brink, Effects of silver nanoparticles

(NM-300K) on *Lumbricus rubellus* erthworms and particle characterization in relevant test matrices including soil, *Environ. Toxicol. Chem*. 2014, **33**, 743-752.

35 P. V. Asharani, Y. Lianwu, Z. Gong, and S. Valiyaveettil, Comparison of the toxicity of silver, gold and platinum nanoparticles in developing zebrafish embryos, *Nanotoxicology,* 2011, **5**, 43-54.

36 J. M. Unrine, S. E. Hunyadi, O. V. Tsyusko, W. Rao, W. A. Shoults-Wilson, and P. M. Bertsch, Evidence for bioavailability of Au nanoparticles from soil and biodistribution within earthworms (*Eisenia fetida*). *Environ. Sci Technol*., 2010, **44**, 8308-83013.

37 C. Lopez-Chaves, J. Soto-Alvaredo, M. Montes-Bayon, J. Bettmer, J. Llopis, and C. Sanchez-Gonzalez, Gold nanoparticles: Distribution, bioaccumulation and toxicity. *In vitro* and *in vivo* studies, *Nanomedicine,* 2018, **14**, 1-12.

38 S. Y. Choi, S. Jeong, S. H. Jang, J. Park, J. H. Park, K. S. Ock, S. Y. Lee, and S. W. Joo, *In vitro* toxicity of serum protein-adsorbed citrate-reduced gold nanoparticles in human lung adenocarcinoma cells. *Toxicol. in vitro*, 2012, **26**, 229-237.

39 H. P. Borase, S. V. Patil, and R. S. Singhal, *Moina macrocopa* as a non-target aquatic organism for assessment of ecotoxicity of silver nanoparticles: effect of size, *Chemosphere*, 2019, **219**, 713-723.

40 B. H. Mao, J. C. Tsai, C. W. Chen, S. J. Yan, and Y. J. Wang, Mechanisms of silver nanoparticle-induced toxicity and important role of autophagy, *Nanotoxicology*, 2016, **10**, 1021-1040.

41 C. S. Patricia, G. V. Nerea, U. Erik, S. M. Elena, B. Eider, D. M. W. Darío, and S. Manu, Responses to silver nanoparticles and silver nitrate in a battery of biomarkers measured in coelomocytes and in target tissues of *Eisenia fetida* earthworms, *Ecotoxicol. Environ. Saf.,* 2017, **141**, 57-63.

42 A. M. Khalil, Physiological and genotoxicological responses of the earthworms *Aporrectodea caliginosa* exposed to sublethal concentrations of AgNPs. *J. Basic & Appl. Zool.,* 2016, **74**, 8–15.

43 M. Novo, E. Lahive, M. Díez-Ortiz, M. Matzke, A. J. Morgan, D. J. Spurgeon, C. Svendsen, and P. Kille, Different routes, same pathways: Molecular mechanisms under silver ion and nanoparticle exposures in the soil sentinel *Eisenia fetida, Environ. Pollut*., 2015, **205**, 385-393.

44 A. H. Ringwood, M. McCarth, T. C. Bates, and D. L. Carroll, The effects of silver nanoparticles on oyster embryos, *Mar. Environ. Res.,* 2010, **69,** S49-51.

45 M. Ahamed, R. Posgai, T. J. Gorey, M. Nielsen, S. M. Hussain, and J. J. Rowe, Silver nanoparticles induced heat shock protein 70, oxidative stress and apoptosis in *Drosophila melanogaster*, *Toxicol. Appl. Pharmacol*., 2010, **242**, 263-269.

46 J. Y. Roh, S. J. Sim, J. Yi, K. Park, K. H. Chung, D. Y. Ryu, and J. Choi, Ecotoxicity of silver nanoparticles on the soil nematode *Caenorhabditis elegans* using functional ecotoxicogenomics, *Environ. Sci. Technol.,* 2009, **43**, 3933-3940.

47 E. Barcinska, J. Wierzbicka, A. Zauszkiewicz-Pawlak, D. Jacewicz, A. Dabrowska, and I. Inkielewicz-Stepniak, Role of oxidative and nitro-oxidative damage in silver nanoparticles cytotoxic effect against human pancreatic ductal adenocarcinoma cells. *Oxid. Med. Cell Longev.,* 2018, **2018**, 8251961.

48 M. Auguste, C. Ciacci, T. Balbi, A. Brunelli, V. Caratto, A. Marcomini, R. Cuppini, and L. Canesi, Effects of nanosilver on *Mytilus galloprovincialis* hemocytes and early embryo development, *Aquatic Toxicol*., 2018, **203**, 107-116.

49 R. Foldbjerg, P. Olesen, M. Hougaard, D. A. Dang, H. J. Hoffmann, and H. Autrup, PVP-coated silver nanoparticles and silver ions induce reactive oxygen species, apoptosis and necrosis in THP-1 monocytes, *Toxicol. Lett.,* 2009, **190**, 156-162.

50 M. Ghooshchian, P. Khodarahmi, and F. Tafvizi, Apoptosis-mediated neurotoxicity and altered gene expression induced by silver nanoparticles, *Toxicol. Ind. Health*, 2017, **33**, 757-764.

51 M. J. Ribeiro, M. J. B. Amorim, and J. J. Scott-Fordsmand, Cell *in vitro* testing with soil invertebrates- challenges and opportunities toward modeling the effect of nanomaterials: a surface-modified CuO case study, *Nanomaterials (Basel),* 2019, **9**, 1087.

52 R. Elespru, S. Pfuhler, M. J. Aardema, T. Chen, S. H. Doak, A. Doherty, C. S. Farabaugh, J. Kenny, M. Manjanatha, B. Mahadevan, M. M. Moore, G. Ouedraogo, L. F. Stankowski, and J. Y. Tanir, Genotoxicity assessment of nanomaterials: recommendations on best practices, assays, and methods, *Toxicol. Sci*., 2018, **164**, 391-416.

53 F. Bernard, F. Brulle, F. Douay, S. Lemière, S. Demuynck, and F. Vandenbulcke, Metallic trace element body burdens and gene expression analysis of biomarker candidates in *Eisenia fetida*, using an "exposure/depuration" experimental scheme with field soils, *Ecotoxicol. Environ. Saf.* 2010, **73**, 1034-1045.

54 N. Asare, N. Duale, H. H. Slagsvold, B. Lindeman, A. K. Olsen, J. Gromadzka-Ostrowska , S. Meczynska-Wielgosz, M. Kruszewski, G. Brunborg, and C. Instanes, Genotoxicity and gene expression modulation of silver and titanium dioxide nanoparticles in mice, *Nanotoxicology*, 2016, **10**, 312-321.

55 Kim, J. E. Choi, J. Choi, K. H. Chung, K. Park, J. Yi, D. and Y. Ryu, Oxidative stress-dependent toxicity of silver nanoparticles in human hepatoma cells, *Toxicol. in vitro* 2009, **23**, 1076–1084.

56 J. M. Njoroge, J. J. Yourick, and M. A. Principato, A flow cytometric analysis of macrophage-nanoparticle interaction *in vitro*: induction of altered Toll-like receptor expression. *Int. J. Nanomedic.* 2018, **13**, 8365-8378.

57 P. Na-Phatthalung, M. Teles, L. Tort, and M. Oliveira, Gold nanoparticles exposure modulates antioxidant and innate immune gene expression in the gills of *Sparus aurata*, *Genomics*, 2018, **110**, 430-434.

58 F. Brulle, G. Mitta, C. Cocquerelle, D. Vieau, S. Lemière, A. Leprêtre, and F. Vandenbulcke, Cloning and real-time PCR testing of 14 potential biomarkers in *Eisenia fetida* following cadmium exposure, *Environ. Sci. Technol.,* 2006, **40**, 2844-2850.

59 G. Tetreau, S. Pinaud, A. Portet, R. Galinier, B. Gourbal, and D. Duval, Specific pathogen recognition by multiple innate immune sensors in an invertebrate, *Front. Immunol.,* 2017, **8**, 1249.

60 A. Alijagic, O. Benada, O. Kofroňová, D. Cigna, and A. Pinsino, Sea urchin extracellular proteins design a complex protein corona on titanium dioxide nanoparticle surface influencing immune cell behaviour, *Front. Immunol*., 2019, **10**, 2261.

61 S. L. Sandiford, Y. Dong, A. Pike, B. J. Blumberg, A. C. Bahia, and G. Dimopoulos, Cytoplasmic actin is an extracellular insect immune factor which is secreted upon immune challenge and mediates phagocytosis and direct killing of bacteria, and is a *Plasmodium* antagonist, *PLoS Pathog*., 2015, **11**, e1004631.

View Article Online
DOI: 10.1039/C9EN01405E

Table 1. Characterization of AgNPs and AuNPs under exposure conditions.

Nominal size	Particle type	Medium	FBS	Characterization data				
				TEM size[a] (nm)	z-average[b] (nm[PdI])	Hydrodynamic size (nm)[c]	ζ potential[d] (mV)	ICP-MS Ion content (mg/L) (%)
10 nm	Ag	RPMI-1640	1%	15. 6 nm ± 7.6	31.4 ± 6.8 [0.186]	37.8 ± 16.5	−9.9 ± 1.1	0.16 (0.4%)
10 nm	Au	RPMI-1640	1%	11. 1 nm ± 4.1	33.8 ± 8.7 [0.265]	45.8 ± 19.8	−13.3 ± 0.8	0.094 (0.24%)

Table 1. Characterization of AgNPs and AuNPs under exposure conditions.
[a]Transmission electron microscopy (TEM); values are mean ± SD, n=300.
[b]Dynamic light scattering; values are z-avarage ± SD; polydispersity index (PdI).
[c]Dynamic light scattering; values are mean ± SD of the particle size distribution obtained by the CONTIN algorithm (shown is the value for the most representative peak).
[d]ζ potential; values are mean ± SD, n=3

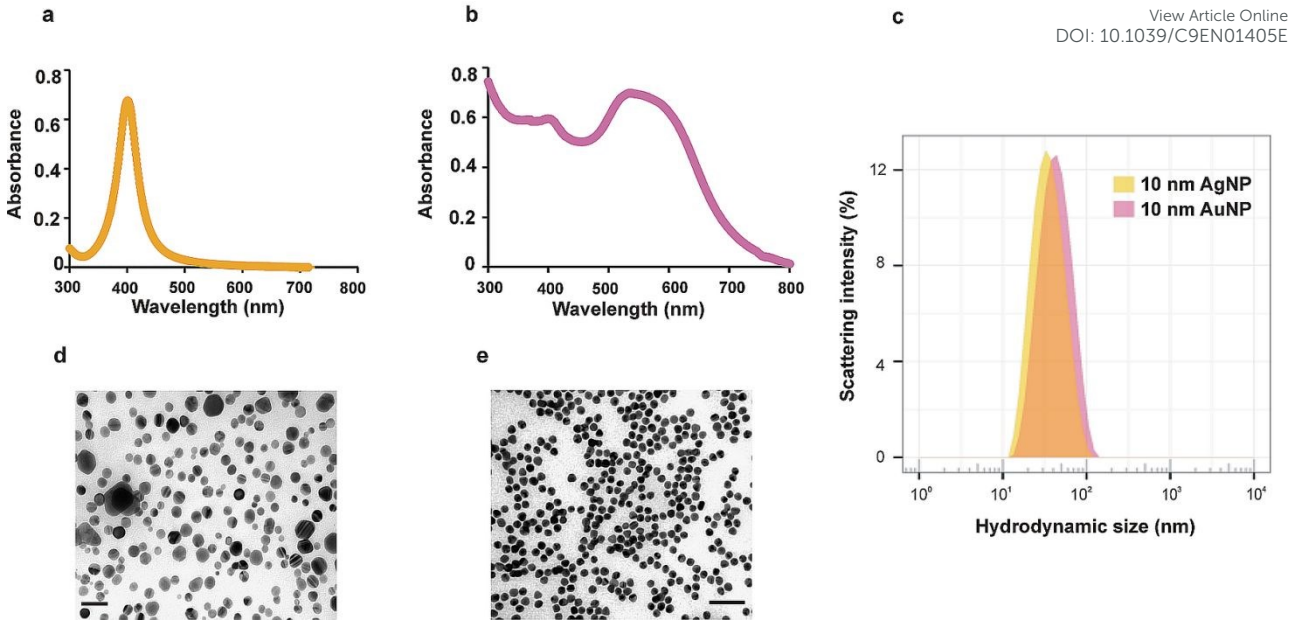

Figure 1. Colloidal stability of 10 nm AgNP and AuNP under exposure conditions. Light absorbance characteristics of localized surface plasmon resonance of 10 nm AgNPs (a) and AuNPs (b) were monitored by spectrophotometry. Representative DLS results showing the scattering intensity-based distribution of hydrodynamic sizes (nm) fitted by the CONTIN algorhitm (c). Primary particle sizes of AgNPs (d) and AuNPs (e) were analyzed by TEM after desalting. Two representative images are presented from three individual experiments, scale bars: 50 nm.

View Article Online
DOI: 10.1039/C9EN01405E

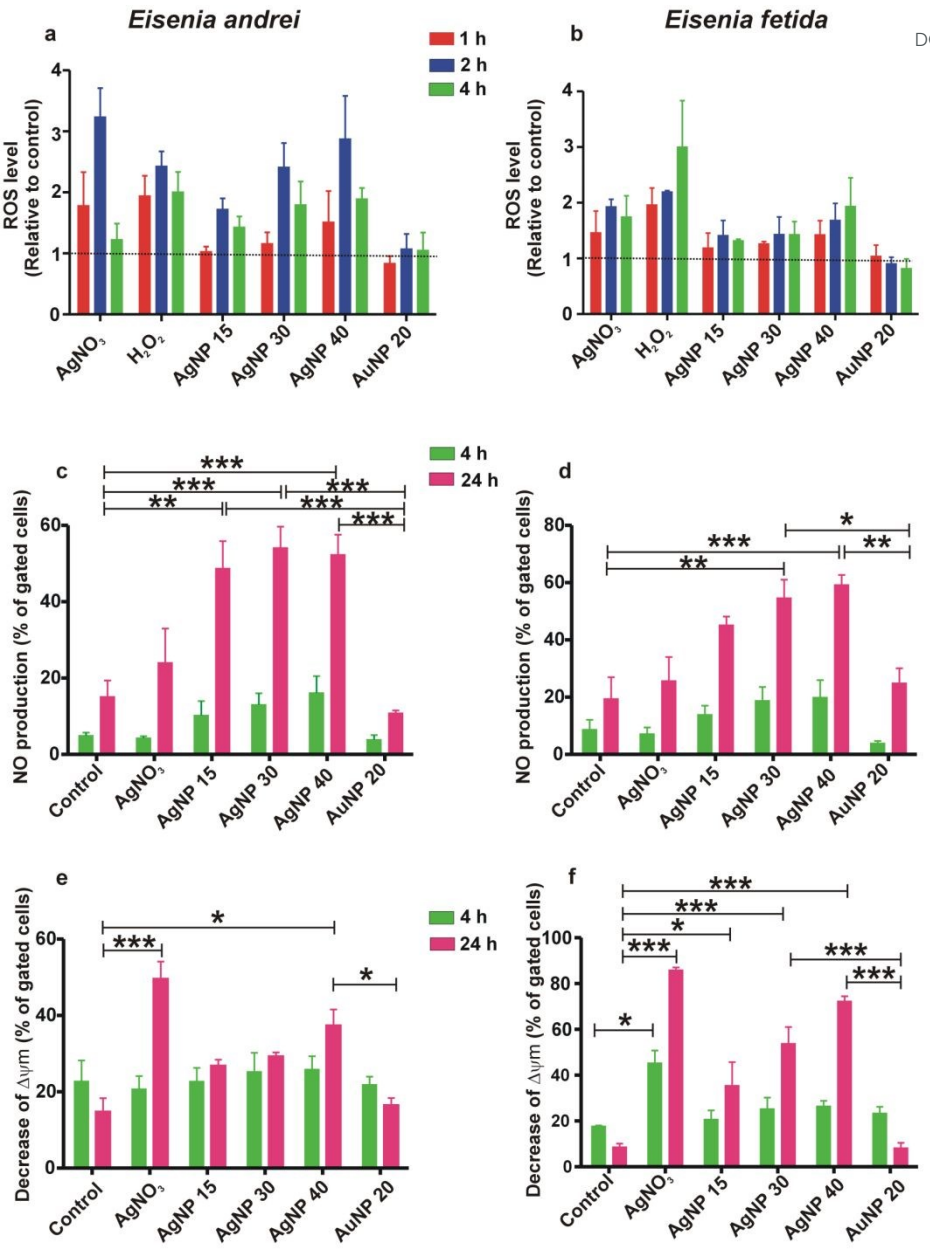

Figure 2. Evaluation of oxidative and mitochondrial stress following exposure to AgNP, AuNP or $AgNO_3$ (1.35 µg/mL). Numbers shown after "AgNP" and "AuNP" refer to the test concentration in µg/mL. Relative ROS levels in the coelomocytes of *E. andrei* (a) and *E. fetida* (b) earthworms over time (1, 2 and 4 h). H_2O_2 served as positive control (100 µM). Dotted lines indicate the basal ROS levels (measured in the control at corresponding time points). Assessment of NO production (% of gated cells) in the coelomocytes of *E. andrei* (c) and *E. fetida* (d) earthworms over time (4 and 24 h). Decrease of mitochondrial membrane

potential (% of gated cells) in *E. andrei* (e) and *E. fetida* (f) coelomocytes over time (4 and 24 h). Three independent measurements (n=3, mean ± SEM) were performed on flow cytometry (FL1 and FL4 filters).

View Article Online
DOI: 10.1039/C9EN01405E

View Article Online
DOI: 10.1039/C9EN01405E

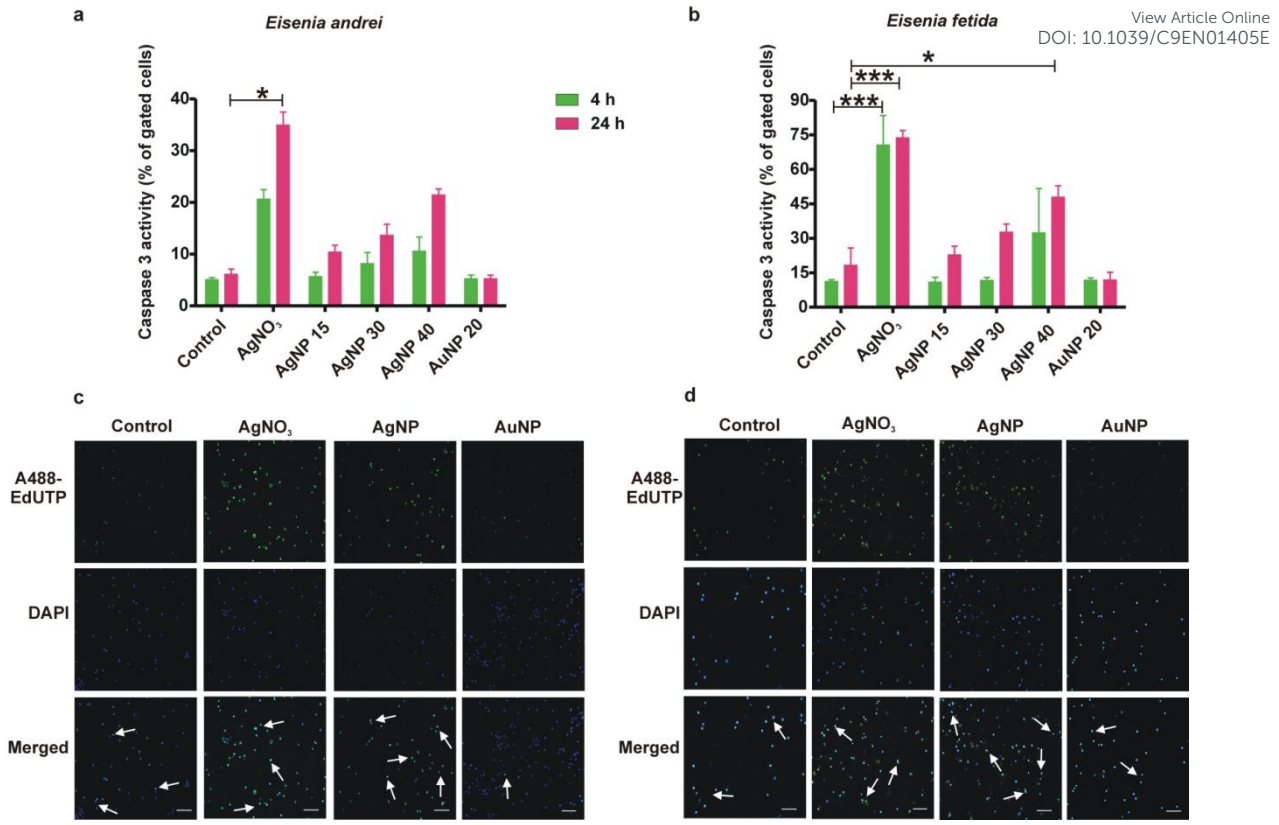

Figure 3. Apoptosis assessment following exposure to AgNP, AuNP or $AgNO_3$ (1.35 µg/mL). Numbers shown after "AgNP" and "AuNP" refer to the test concentration in µg/mL. Flow cytometry-based caspase-3 activity (% of gated cells) in coelomocytes of *E. andrei* (a) and *E. fetida* (b) over time (4 h and 24 h). Representative TUNEL-assay images of control (ddH_2O), $AgNO_3$ (1.35 µg/mL), AgNP (40 µg/mL) and AuNP (20 µg/mL) exposed coelomocytes of *E. andrei* (c) and *E. fetida* (d) earthworms are shown, scale bars: 50 µm. Each measurements were conducted three times (n=3), results are represented as mean ± SEM.

View Article Online
DOI: 10.1039/C9EN01405E

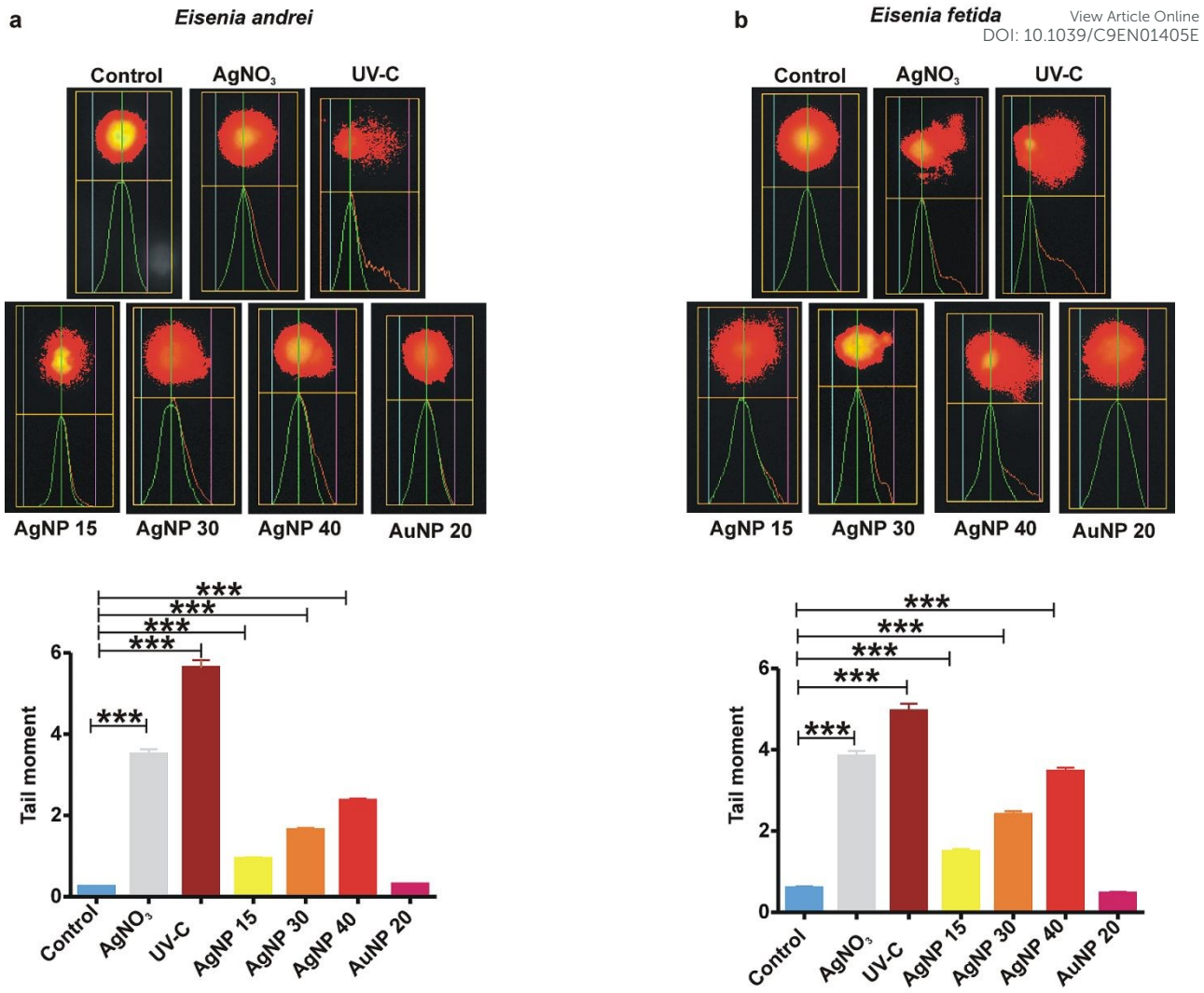

Figure 4. Degree of DNA-damage following 24 h exposure to AgNP, AuNP or $AgNO_3$ (1.35 µg/mL). Numbers shown after "AgNP" and "AuNP" refer to the test concentration in µg/mL. Comet-assay was performed in coelomocytes of *E. andrei* (a) and *E. fetida* (b). UV-C treatment served as a positive control. Representative images from one Comet-assay are shown in the top panel. Blue lines show the "front of the head", green lines the "middle of the cells" and purple lines the "end of the tail". Each treatment was independently performed three times (n=3), and in one experiment at least 80 cells were evaluated. Graphs in the bottom panels demonstrate "Tail-moment" values with standard error of the mean (±SEM).

View Article Online
DOI: 10.1039/C9EN01405E

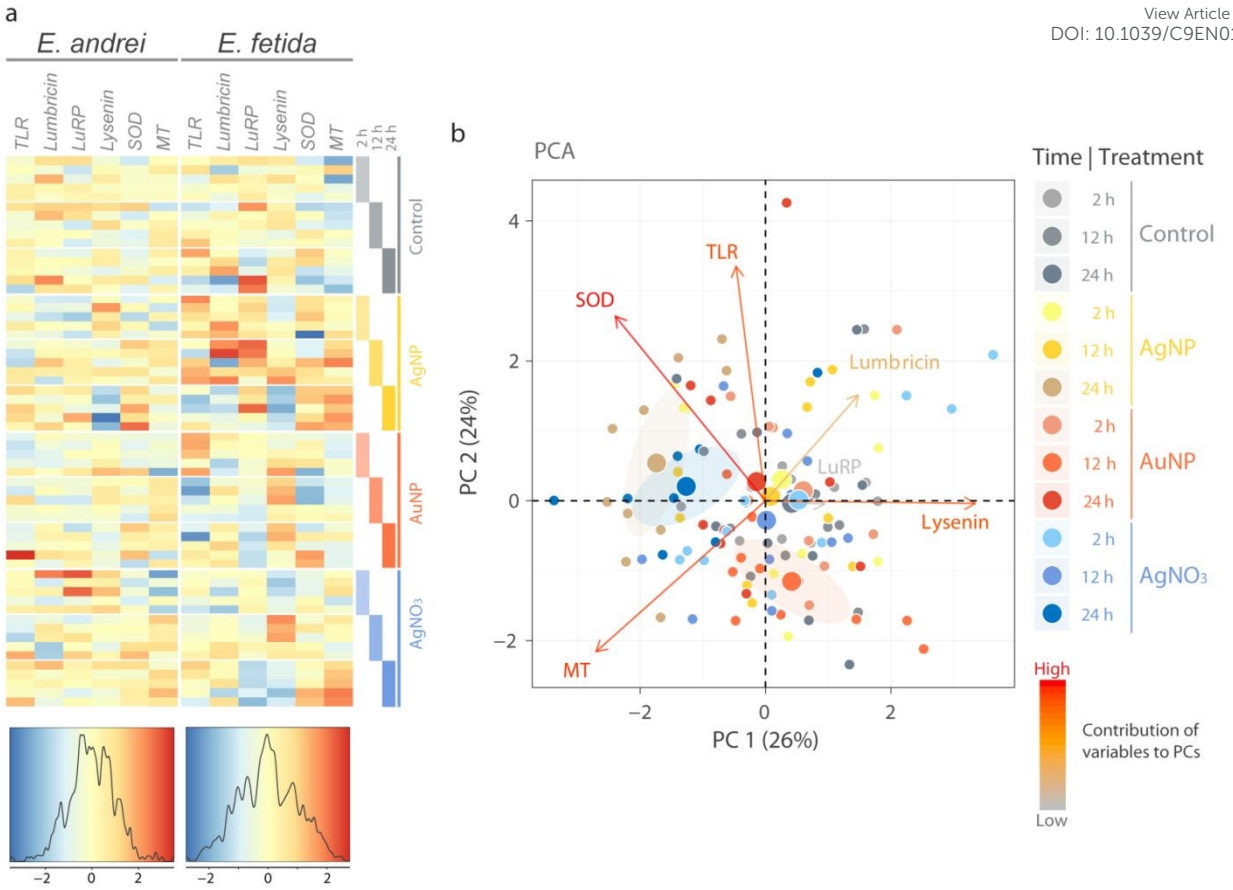

Figure 5. Heatmap and principal component analysis (PCA). The relative gene expression values are shown as a heatmap for each species along with the z-score density and a color key. Sample features are color-coded and each treatment is split into three groups (2, 12 and 24 h) consisting of 5 biological replicates (a). PCA biplot is shown for the species-pooled dataset. Individual samples (small dots) and mean points (large dots) are plotted according to the coordinates in the first two PCs, overlaid with variable coefficients (arrows). Contributions of the 6 variables (genes) to the two PCs are color-scaled from grey to red. Confidence ellipses are drawn for sample features that on average have greater PC scores than the rest of the samples (b).

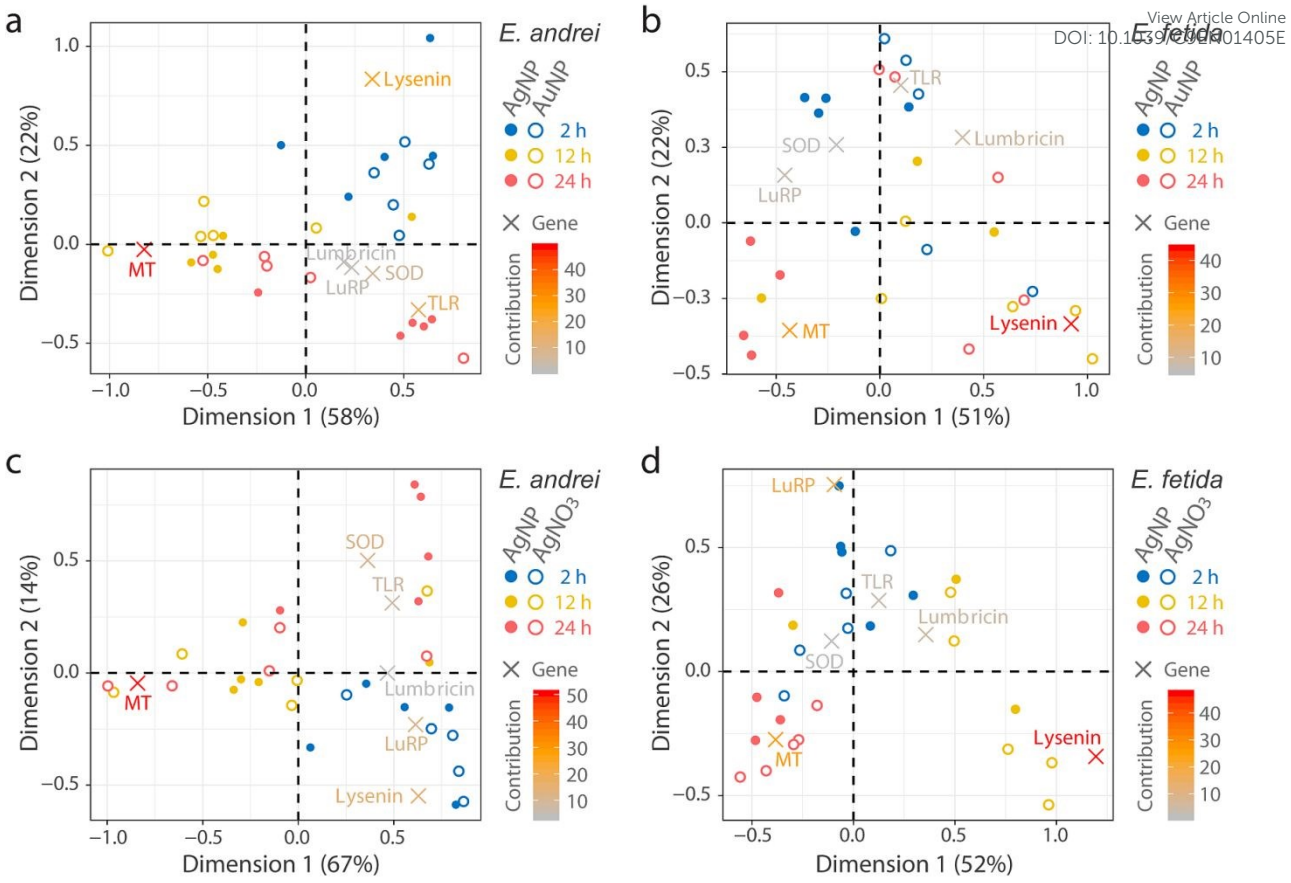

Figure 6. Correspondence analysis (CA). CA biplots for the temporal gene expression profiles are shown in a combination of AgNP and AuNP (a, b) or AgNP and $AgNO_3$ (c, d) for the two species, respectively. Individual samples (small dots or circles) and genes (crosses) are plotted according to the coordinates in the first two dimensions. Contributions of the 6 variables (genes) to the two dimensions are color-scaled from gray to red. Dots/circles (expression profiles at the specified time point) in the proximity of a cross (gene) signify an association between the exposure time and the transcriptional response, and its relative importance is determined by the contribution of the gene to each dimension. Three outlier samples were excluded from the AgNP dataset for *E. fetida* (2 replicates for the 12 h time point and 1 replicate for the 24 h time point), as they had predominant levels of *LuRP* expression affecting the analysis overall (b, d).

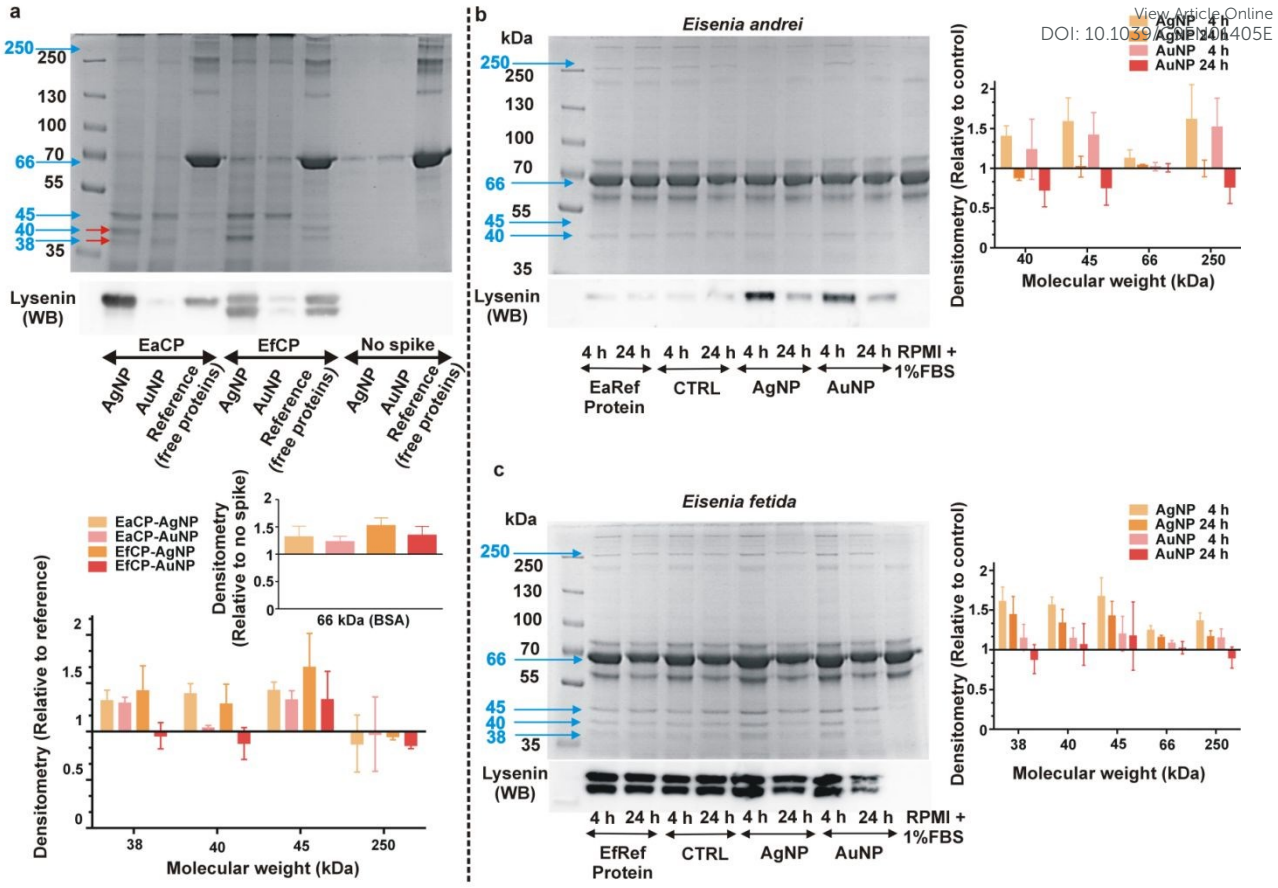

Figure 7. *Ex-situ* protein corona formation (a) and protein secretion profile of coelomocytes from *E. andrei* (b) and *E. fetida* (c) earthworms studied by SDS-PAGE and Coomasssie Brilliant Blue staining or Western blotting of lysenins. Representative gels from three independent experiments are shown. Red arrows indicate the members of the lysenin-protein family, supposedly lysenin (lower arrow) and lysenin-related protein 2 (top arrow) identified by LC-MS/MS. Blue arrows indicate lysenin (~37-38 kDa), lysenin-related protein 2 (~40 kDa), other corona proteins (~45 kDa, >200 kDa) and BSA (~66 kDa). The associated graphs show the enrichment of these bands calculated as the band intensity normalized to the corresponding protein band in the reference protein lanes (a) or in the control lanes (b, c). The values are mean ± SEM. Protein corona profiles for AgNPs and AuNPs following 24 h incubation in CP-spiked cell culture media supplemented with BSA as a background protein source (a). Protein secretion profiles of *E. andrei* (b) and *E. fetida* coelomocytes (c) exposed to low-cytotoxic concentration of AgNP (*E. andrei*: 2.71 µg/mL, *E. fetida*: 2 µg/mL) and AuNP (20 µg/mL). A blank (RPMI+1% FBS) is included showing serum proteins without coelomocytes. Western-blot analysis verified the dynamic changes of lysenin and lysenin-related peptide (LRP) secretion upon NP exposure.

ToC Entry

This study is focused on the remarkable sensitivity differences of immune cells from two closely-related earthworm species (*Eisenia andrei* and *E. fetida)* towards noble metal nanomaterials at cellular and molecular levels.